Pramana – J. Phys. (2019) 93:62
https://doi.org/10.1007/s12043-019-1815-2

Transportation of activation energy in the Oldroyd-B nanofluid by considering double stratification over a surface with variable thickness

M IJAZ KHAN[1,*], SUMAIRA QAYYUM[1], SHAHID FAROOQ[1], T HAYAT[1,2] and A ALSAEDI[2]

[1]Department of Mathematics, Quaid-I-Azam University 45320, Islamabad 44000, Pakistan
[2]Nonlinear Analysis and Applied Mathematics (NAAM) Research Group, Department of Mathematics, Faculty of Science, King Abdulaziz University, P.O. Box 80257, Jeddah 21589, Saudi Arabia
*Corresponding author. E-mail: mikhan@math.qau.edu.pk

MS received 28 July 2018; revised 25 February 2019; accepted 25 March 2019

Abstract. In this communication, the impact of activation energy on the nonlinear binary chemically reactive flow of an Oldroyd-B nanofluid has been examined. Buongiorno's nanofluid model is used in mathematical modelling. The flow behaviour is discussed over a nonlinear stretchable surface with variable thickness. Nonlinear mixed convection is considered. The energy equation is modelled subject to a heat source/sink and radiative flux. Furthermore, double stratification at the boundary of the sheet is considered for the heat and mass transfers. Important slip mechanisms such as Brownian and thermophoresis diffusions are accounted. The obtained flow expressions are analytically solved by using the optimal homotopy asymptotic method (OHAM). Computational analysis for concentration, temperature and velocity is obtained and discussed using plots. Nusselt and Sherwood numbers are discussed using a tabulated form. Total squared residual error is calculated for velocity, temperature and concentration. The obtained results show that for increased values of Hartmann (magnetic parameter) and Deborah numbers, the fluid velocity decreases. The temperature field shows an increasing impact in the presence of larger radiative parameters. Sherwood and Nusselt numbers increase with higher values of thermophoresis and solutal stratified parameters.

Keywords. Activation energy; chemical reaction; radiative flux; Oldroyd-B nanofluid; heat generation/absorption; stratification for heat and mass at the boundary.

PACS Nos **44.25.+f; 47.10.A; 47.10.ad; 47.15.G; 47.27.Ak**

1. Introduction

Energy demand in the mechanical and the industrial engineering process is increasing rapidly. As it is difficult to decrease the power consumption, the execution of heat transfer by a device is of extraordinary significance. But the conventional pure liquid heat transport medium cannot meet the requirements under some extraordinary working conditions. It is important to develop effective heat transport medium. Nanoliquids, which were initially proposed by Lee *et al* [1], are another type of working liquid. The development of nanoliquids in the past two decades makes nanoliquids a notably efficient working liquid. Nanoliquids have been taken as another type of cooling medium to enhance heat transport [2]. Numerous investigations have been conducted to enhance heat transport qualities of nanoliquids. The results demonstrated that besides enhancing thermal conductivity, the adjustment in the flow features by the interaction between the nanomaterials and base liquid is another factor that influences the heat transfer by nanoliquids. Accordingly, it is important to explore the flow attributes of nanoliquids. Zhang *et al* [3], Cui *et al* [4] and Zhang *et al* [5] explored the reason as to why nanoliquids can strengthen the heat transport. The experimental outcomes demonstrated that the interaction between the base liquid and nanomaterials had changed the flow characteristics, which upgraded the mass and heat transfers. Laein *et al* [6] estimated the laminar boundary layer thickness of TiO_2–water nanoliquids under natural convection state through particle image velocimetry (PIV). The obtained results demonstrated that the layer thickness significantly decreased after the addition of nanomaterials, thus increasing the

Published online: 18 July 2019

heat transport. Different studies on different flow models and flow assumptions are listed in [7–20].

Motivated by some of the investigators and researchers referenced above and their applications in different fields of mechanical and industrial engineering, it is important to study and examine the impact of activation energy and double stratification effects on the binary chemically reactive flow of the Oldroyd-B nanofluid over a stretchable surface with variable thickness. A majority of the articles in the literature revealed, on similarity solutions, free convections, heat and mass transport through a porous medium and a semianalytical solution through the homotopy method [21–25], built-in shooting method [26–30], Bvp4c method [31–35], Akbari–Ganji method [36–40], etc. But in the present article, the governing flow expressions are analytically tackled by the optimal homotopy asymptotic method (OHAM) [41–45] with the help of similarity transformations.

2. Mathematical description

Here, the impact of activation energy in the nanomaterial flow of the Oldroyd-B fluid is discussed. The applied magnetic field is considered. Flow behaviour is examined over a surface of a sheet with variable thicknesses. Furthermore, nonlinear mixed convection, radiative flux and heat source/sink effects are also considered. The magnetic field strength and heat generation coefficient are taken as $B(x) = B_0(x+b)^{(n-1)/2}$ and $Q(x) = Q_0(x+b)^{n-1}$, respectively. Brownian and thermophoresis diffusion effects are accounted. Figure 1 is modelled for the physical analysis of the flow.

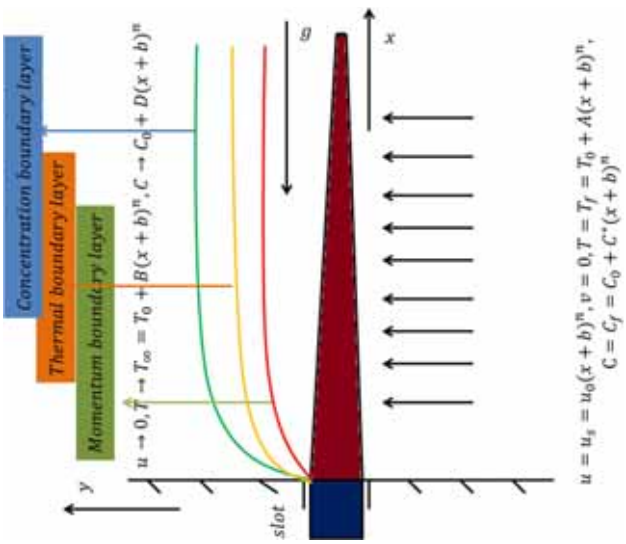

Figure 1. Schematic flow diagram.

The nonlinear flow equations in component form are

$$\frac{\partial u}{\partial x}+\frac{\partial v}{\partial y}=0, \tag{1}$$

$$\left.\begin{aligned} u\frac{\partial u}{\partial x}+v\frac{\partial u}{\partial y}&=\nu\frac{\partial^2 u}{\partial y^2}+\lambda_1\left(u^2\frac{\partial^2 u}{\partial x^2}+v^2\frac{\partial^2 u}{\partial y^2}\right.\\ &\left.+2uv\frac{\partial^2 u}{\partial x\partial y}\right)+\nu\lambda_2\left(u\frac{\partial^3 u}{\partial x\partial y^2}+v\frac{\partial^3 u}{\partial y^3}\right.\\ &\left.-\frac{\partial u}{\partial x}\frac{\partial^2 u}{\partial y^2}+\frac{\partial u}{\partial y}\frac{\partial^2 u}{\partial x\partial y}\right)-\frac{\sigma}{\rho}B^2\left(u+\lambda_1 v\frac{\partial u}{\partial y}\right)\\ &+g\{\alpha_1(T-T_\infty)+\alpha_2(T-T_\infty)^2\}\\ &+g\{\alpha_3(C-C_\infty)+\alpha_4(C-C_\infty)^2\}\end{aligned}\right\}, \tag{2}$$

$$\left.\begin{aligned} u\frac{\partial T}{\partial x}+v\frac{\partial T}{\partial y}&=\frac{k}{(\rho c)_f}\frac{\partial^2 T}{\partial y^2}\\ &+\tau\left(D_{\mathrm{B}}\frac{\partial C}{\partial y}\frac{\partial T}{\partial y}+\frac{D_T}{T_\infty}\left(\frac{\partial T}{\partial y}\right)^2\right)\\ &+\frac{1}{(\rho c)_f}\frac{16\sigma^* T_\infty^3}{3k^*}\frac{\partial^2 T}{\partial y^2}+\frac{Q(x)}{(\rho c)_{\mathrm{f}}}(T-T_\infty)\end{aligned}\right\}, \tag{3}$$

$$u\frac{\partial C}{\partial x}+v\frac{\partial C}{\partial y}=D_{\mathrm{B}}\frac{\partial^2 C}{\partial y^2}+\frac{D_{\mathrm{T}}}{T_\infty}\frac{\partial^2 T}{\partial y^2}$$

$$-k_r^2(C-C_\infty)\left(\frac{T}{T_\infty}\right)^m\exp\left(-\frac{E_{\mathrm{a}}}{\kappa T}\right) \tag{4}$$

with boundary conditions

$$\left.\begin{aligned} &u=u_{\mathrm{s}}=u_0(x+b)^n,\quad v=0,\\ &T=T_{\mathrm{f}}=T_0+A(x+b)^n\\ &C=C_{\mathrm{f}}=C_0+C^*(x+b)^n\\ &\text{at } y=A_1(x+b)^{(1-n)/2}\\ &u=0,\ T\to T_\infty=T_0+B(x+b)^n,\\ &C\to C_\infty=C_0+D(x+b)^n\quad \text{at } y\to\infty\end{aligned}\right\}. \tag{5}$$

In the above expressions, x, y indicate the Cartesian coordinates, u, v are the velocity components, λ_1, λ_2 are the relaxation and retardation times, respectively, ν is the kinematic viscosity, σ is the electrical conductivity, ρ is the density, B_0 is the strength of the magnetic field, $\alpha_1, \alpha_2, \alpha_3, \alpha_4$ highlight the thermal and concentration expansion coefficients in linear and nonlinear forms, g is the gravitational acceleration, T is the temperature, k is the thermal conductivity, T_∞ is the ambient temperature, σ^* is the Stefan–Boltzmann constant, C is the concentration, k^* is the mean absorption coefficient, C_∞ is the ambient concentration and c_p is the

specific heat, $\tau\left(=(\rho c)_p/(\rho c)_f\right)$ represents the ratio of the heat capacities of the fluid and the nanomaterials, k_r^2 is the reaction rate coefficient, D_{B} is the Brownian diffusion coefficient, m is the fitted rate constant, D_{T} is the thermophoresis diffusion, Q is the heat generation coefficient, κ is the Boltzmann constant, E_{a} is the activation energy coefficient, n is the power index, C_0, T_0 respectively are the reference concentration and temperature, A, B, C^*, D are dimensional constants, T_f, C_f are respectively the fluid temperature and concentration and u_{s} denotes the stretching velocity.

Considering

$$\left.\begin{aligned} u &= u_0(x+b)^n F'(\eta)\\ v &= -\sqrt{\frac{\nu u_0(n+1)(x+b)^{n-1}}{2}}\\ &\quad\times\left(F(\eta)+\xi\frac{n-1}{n+1}F'(\eta)\right)\\ \eta &= \sqrt{\frac{u_0(n+1)}{2\nu}}y(x+b)^{(n-1)/2}\\ \psi &= \sqrt{\frac{2\nu u_0(x+b)^{n+1}}{n+1}}F(\eta)\\ \theta(\eta) &= \frac{T-T_\infty}{T_f-T_0},\ \varphi(\eta)=\frac{C-C_\infty}{C_{\mathrm{f}}-C_0} \end{aligned}\right\} \tag{6}$$

we have

$$\left.\begin{aligned} &F'''+F''F-\frac{2n}{n+1}\left(F'\right)^2+\beta_1((3n-1)FF'F''\\ &-\frac{2n(n-1)}{n+1}\left(F'\right)^3-\frac{n+1}{2}F^2F'''\\ &+\xi\frac{n-1}{2}F''\left(F'\right)^2+\xi\frac{n-1}{2}F''\left(F'\right)^2)\\ &+\beta_2\left(\frac{n-1}{2}F'F^3+\frac{3n-1}{2}\left(F''\right)^2\right.\\ &\left.-\frac{n+1}{2}FF^{iv}\right)-\frac{2M}{n+1}F'\\ &+M\beta_1\left(FF''+\xi\frac{n-1}{n+1}F'F''\right)\\ &+\frac{2\Lambda_T}{n+1}\left[(1+\beta_{\mathrm{T}}\Theta)\Theta+N^*(1+\beta_{\mathrm{C}}\Phi)\Phi\right]=0 \end{aligned}\right\}, \tag{7}$$

$$\begin{aligned} &\frac{1}{\mathrm{Pr}}\left[1+R(\theta_w)^3\right]\Theta''-\frac{2n}{n+1}\left(F'\Theta+F'S_1\right)+F\Theta'\\ &+N_b\Theta'\Phi'+N_t\left(\Theta'\right)^2+\frac{2}{n+1}\delta\Theta=0, \end{aligned} \tag{8}$$

$$\begin{aligned} &\Phi''+\frac{N_t}{N_b}\Theta''+\mathrm{Sc}F\Phi'-\frac{2\mathrm{Sc}n}{n+1}\left(F'\Phi+F'S_2\right)\\ &-\mathrm{Sc}\gamma\left(1+\delta^*\Theta\right)^m\Phi\exp\left(\frac{-E_1}{1+\delta^*\Theta}\right)=0 \end{aligned} \tag{9}$$

with

$$\left.\begin{aligned} &F'(\alpha)=1,\ F(\alpha)=\frac{\alpha(1-n)}{1+n},\ F'(\infty)=0\\ &\Theta'(\alpha)=(1-S_1),\ \Theta(\infty)=0\\ &\Phi'(\alpha)=(1-S_2),\ \Phi(\infty)=0 \end{aligned}\right\}. \tag{10}$$

Here $\beta_1\left(=\lambda_1u_0(x+b)^{n-1}\right)$ and $\beta_2\left(=\lambda_2u_0(x+b)^{n-1}\right)$ designate the Deborah numbers in terms of relaxation and retardation parameters, $M\left(=\sigma B_0^2/\rho u_0\right)$ represents the magnetic parameter, $\mathrm{Pr}(=\nu/\alpha^*)$ is the Prandtl number, $\mathrm{Sc}(=\nu/D_{\mathrm{B}})$ is the Schmidt number, $N^*\left(=G_r^*/G_r\right)$ represents the ratio of thermal and concentration forces, $N_t\left(=\tau D_{\mathrm{T}}(T_f-T_0)/\nu T_\infty\right)$ is the thermophoresis variable, $R\left(=16\sigma^*T_\infty^3/3k^*k\right)$ is the radiation parameter, $N_b\left(=\tau D_{\mathrm{B}}\left(C_f-C_0\right)/\nu\right)$ is the Brownian diffusion variable, $\theta_w(=T_\infty/T_0)$ is the temperature ratio, $\Lambda_{\mathrm{T}}(=G_r/(\mathrm{Re}_{xy})^2)$ is the mixed convection variable, $\gamma(=k_r^2/u_0)$ is the chemical reaction variable, $\beta_{\mathrm{T}}(=\alpha_2(T_f-T_0)/\alpha_1)$ is the nonlinear thermal convective variable, $E_1(=E_{\mathrm{a}}/\kappa T_\infty)$ is the activation variable, $\beta_{\mathrm{C}}\left(=\alpha_4\left(C_f-C_0\right)/\alpha_3\right)$ is the nonlinear concentration convective variable, $\delta\left(=Q_0/(\rho c)_f u_0\right)$ is the heat generation variable, $\delta^*(=(T_w-T_\infty)/T_\infty)$ is the temperature ratio variable and $S_1(=T_1/T_2)$, $S_2(=C_1/C_2)$ are the thermal and solutal stratified variables.

Now setting $F(\eta)=f(\eta-\alpha)=f(\xi)$, $\Theta(\eta)=\theta(\eta-\alpha)=\theta(\xi)$, $\Phi(\eta)=\phi(\eta-\alpha)=\phi(\xi)$, one has

$$\left.\begin{aligned} &f'''+f''f-\frac{2n}{n+1}\left(f'\right)^2+\beta_1((3n-1)ff'f''\\ &-\frac{2n(n-1)}{n+1}\left(f'\right)^3-\frac{n+1}{2}f^2f'''\\ &+\xi\frac{n-1}{2}f''\left(f'\right)^2)+\beta_2\left(\frac{n-1}{2}f'f^3\right.\\ &\left.+\frac{3n-1}{2}\left(f''\right)^2-\frac{n+1}{2}ff^{(iv)}\right)-\frac{2M}{n+1}f'\\ &+M\beta_1\left(ff''+\xi\frac{n-1}{n+1}f'f''\right)\\ &+\frac{2\Lambda_{\mathrm{T}}}{n+1}\left[(1+\beta_{\mathrm{T}}\theta)\theta+N^*(1+\beta_{\mathrm{C}}\phi)\phi\right]=0, \end{aligned}\right\}. \tag{11}$$

$$\begin{aligned} &\frac{1}{\mathrm{Pr}}\left(1+R\theta_w^3\right)\theta''+f\theta'-\frac{2n}{n+1}\left(f'\theta+f'S_1\right)\\ &+N_b\theta'\phi'+N_t\left(\theta'\right)^2+\frac{2}{n+1}\delta\theta=0, \end{aligned} \tag{12}$$

$$\begin{aligned} &\phi''+\frac{N_t}{N_b}\theta''+\mathrm{Sc}f\varphi'-\frac{2n\mathrm{Sc}}{n+1}\left(f'\phi+f'S_2\right)\\ &-\mathrm{Sc}\gamma\left(1+\delta^*\theta\right)^m\phi\exp\left(\frac{-E_1}{1+\delta^*\theta}\right)=0 \end{aligned} \tag{13}$$

with

$$\left.\begin{array}{l} f'(0)=1, \quad f(0)=\dfrac{\alpha(1-n)}{1+n}, \quad f'(\infty)=0 \\ \theta'(0)=(1-S_1), \quad \theta(\infty)=0 \\ \phi'(0)=1-S_2, \quad \phi(\infty)=0 \end{array}\right\}. \tag{14}$$

3. Engineering quantities

3.1 *Nusselt number*

We have

$$\mathrm{Nu}_x=\frac{(x+b)q_w}{k\left(T_f-T_\infty\right)}, \tag{15}$$

where q_w indicates the wall heat flux and is defined as

$$q_s=-k\left(1+\frac{16\sigma^* T_\infty^3}{3kk^*}\right) \times\left(\frac{\partial T}{\partial y}\right)\Big|_{y=A_1(x+b)^{(1-n)/2}}. \tag{16}$$

Finally, one has

$$\mathrm{Nu}_x\mathrm{Re}_x^{-0.5}=-\frac{1}{1-S_1}\sqrt{\frac{n+1}{2}}\left(1+R\theta_w^3\right)\theta'(0). \tag{17}$$

3.2 *Sherwood number*

Mathematically, it is expressed as

$$\mathrm{Sh}_x=\frac{(x+b)q_m}{D_\mathrm{B}\left(C_f-C_\infty\right)}, \tag{18}$$

where q_m represents the wall mass flux and it is addressed as

$$q_m=-D_\mathrm{B}\left[\frac{\partial C}{\partial y}\right]\Big|_{y=A_1(x+b)^{(1-n)/2}}. \tag{19}$$

In the dimensionless form, one has

$$\mathrm{Sh}_x\mathrm{Re}_x^{-0.5}=-\frac{1}{1-S_2}\sqrt{\frac{n+1}{2}}\varphi'(0), \tag{20}$$

where $\mathrm{Re}_x\left(=(u_0/\nu)(x+b)^{n+1}\right)$ highlights the local Reynolds number.

4. Solution methodology

Here, we have used the OHAM [45] to solve the nonlinear flow expressions. Therefore, the initial approximations and linear operators are expressed as

$$\left.\begin{array}{l} f_0(\xi)=\alpha\left(\dfrac{1-n}{1+n}\right)+1-\exp(-\eta) \\ \theta_0(\xi)=(1-S_1)\exp(-\eta) \\ \phi_0(\xi)=(1-S_2)\exp(-\eta) \end{array}\right\}. \tag{21}$$

$$\left.\begin{array}{l} \pounds_f(f)=\dfrac{\mathrm{d}^3 f}{\mathrm{d}\xi^3}-\dfrac{\mathrm{d}f}{\mathrm{d}\xi} \\ \pounds_\theta(\theta)=\dfrac{\mathrm{d}^2\theta}{\mathrm{d}\xi^2}-\theta \\ \pounds_\varphi(\phi)=\dfrac{\mathrm{d}^2\varphi}{\mathrm{d}\xi^2}-\phi \end{array}\right\}, \tag{22}$$

with the characteristics

$$\left.\begin{array}{l} L_f\left[A_1^*+A_2^*\exp(\xi)+A_3^*\exp(-\xi)\right]=0 \\ L_\theta\left[A_4^*\exp(\xi)+A_5^*\exp(-\xi)\right]=0 \\ L_\phi\left[A_6^*\exp(\xi)+A_7^*\exp(-\xi)\right]=0 \end{array}\right\}, \tag{23}$$

where A_i $(i=1{-}7)$ highlights the arbitrary constants.

5. Convergence analysis through the OHAM

In the OHAM, the auxiliary variables play a significant role in the convergence region. Liao [45] used the idea of minimisation which represents the average squared residual errors for $\hbar_f$, $\hbar_\theta$ and $\hbar_\phi$. Mathematically, it is expressed as

$$e_{m^{**}}^f=\frac{1}{k^{**}+1}\sum_{j=0}^{k^{**}}\left[N_f\left(\sum_{j=0}^{m^{**}}(f_j)_{\xi=j\delta\eta}, \sum_{j=0}^{m^{**}}(\theta_j)_{\xi=j\delta\eta}, \sum_{j=0}^{m^{**}}(\phi_j)_{\xi=j\delta\eta}\right)\right]^2, \tag{24}$$

$$e_{m^{**}}^f=\frac{1}{k^{**}+1}\sum_{j=0}^{k^{**}}\left[N_\theta\left(\sum_{j=0}^{m^{**}}(f_j)_{\xi=j\delta\eta}, \sum_{j=0}^{m^{**}}(\theta_j)_{\xi=j\delta\eta}, \sum_{j=0}^{m^{**}}(\phi_j)_{\xi=j\delta\eta}\right)\right]^2, \tag{25}$$

$$e_{m^{**}}^f=\frac{1}{k^{**}+1}\sum_{j=0}^{k^{**}}\left[N_\phi\left(\sum_{j=0}^{m^{**}}(f_j)_{\xi=j\delta\eta}, \sum_{j=0}^{m^{**}}(\theta_j)_{\xi=j\delta\eta}, \sum_{j=0}^{m^{**}}(\phi_j)_{\xi=j\delta\eta}\right)\right]^2. \tag{26}$$

Table 1. Individual iterations of residual errors using auxiliary variables.

m^{**}	$e^{f}_{m^{**}}$	$e^{\theta}_{m^{**}}$	$e^{\phi}_{m^{**}}$
2	2.11505×10^{-6}	0.0229805	0.0759172
8	1.36149×10^{-7}	0.00275001	0.0122751
10	9.11568×10^{-8}	0.00176796	0.00886119
16	3.86652×10^{-8}	0.000641828	0.00428537

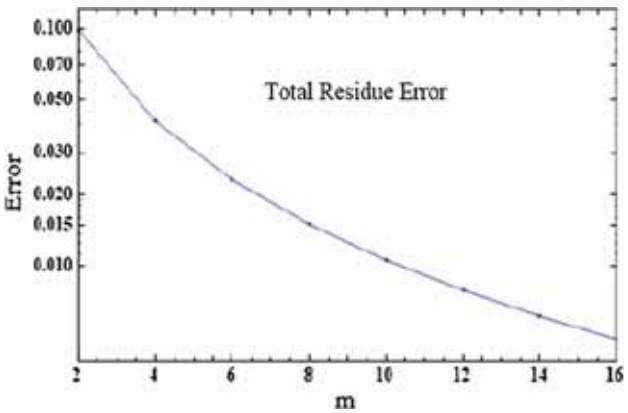

Figure 2. Total residual error.

Following Liao [45]:

$$e^{t}_{m^{**}} = e^{f}_{m^{**}} + e^{\theta}_{m^{**}} + e^{\phi}_{m^{**}}, \tag{27}$$

where $e^{t}_{m^{**}}$ illustrates the total residual squared error, $\delta\eta = 0.5$ and $k = 20$. The numerical values of auxiliary variables at second iterations are $\hbar_f = -1.34317$, $\hbar_\theta = -0.298064$, $\hbar_\phi = -1.34541$ and $e^{t}_{m^{**}} = 0.0988998151$. Furthermore, table 1 is plotted for the individual average residual error of velocity, temperature and concentration utilising auxiliary variables at $m^{**} = 2$. From the obtained outcomes, it is noticed that the residual error displays a reducing trend via higher iterations.

6. Discussion

In this section, we have presented the graphical outcomes of various pertinent variables like Deborah number with respect to relaxation and retardation times (β_1, β_2), Hartmann number (M), radiation parameter (R), solutal and thermal stratification parameters (S_1, S_2), Prandtl number (Pr), thermophoresis parameter (N_t) and activation variable (E_1) on the flow field, temperature, concentration and Nusselt and Sherwood numbers. Figure 1 depicts the graphical sketch of flow analysis. Figure 2 highlights the average residual error with the help of an auxiliary variable. Table 1 represents the individual residual error for the velocity, temperature and concentration fields using auxiliary variables.

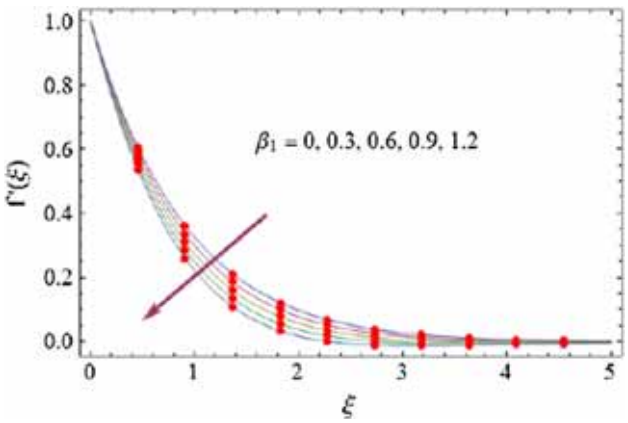

Figure 3. Impact of Deborah number (β_1) on velocity.

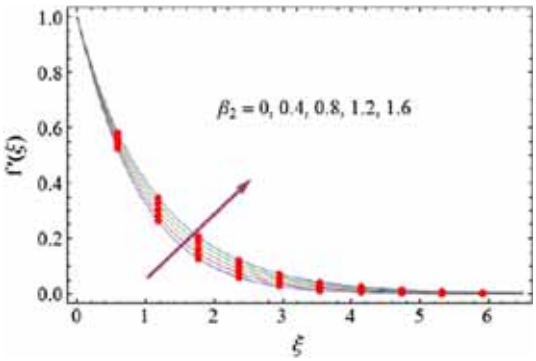

Figure 4. Impact of Deborah number (β_2) on velocity.

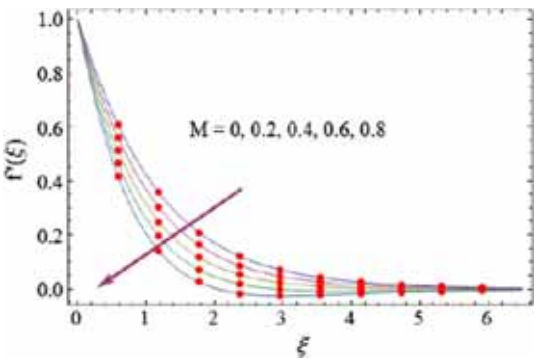

Figure 5. Impact of Hartman number (M) on velocity.

Figures 3–14 are sketched to indicate the impact of velocity, temperature, concentration, Nusselt number and Sherwood number on the dimensionless variables involved in the analysis. A decreasing trend is noticed for the velocity field $\left(f'(\xi)\right)$ for higher values of Deborah number with respect to relaxation time ($\beta_1 = 0, 0.3, 0.6, 0.9, 1.2$) (see figure 3). Physically,

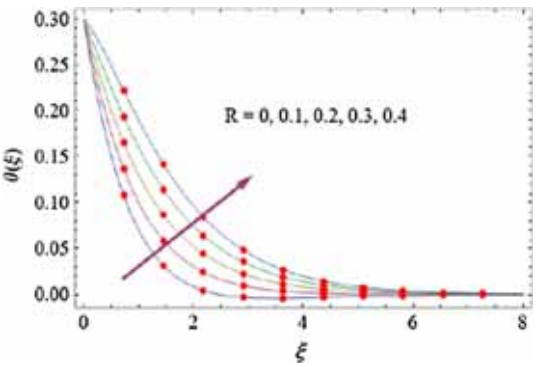

Figure 6. Impact of radiation parameter (R) on temperature.

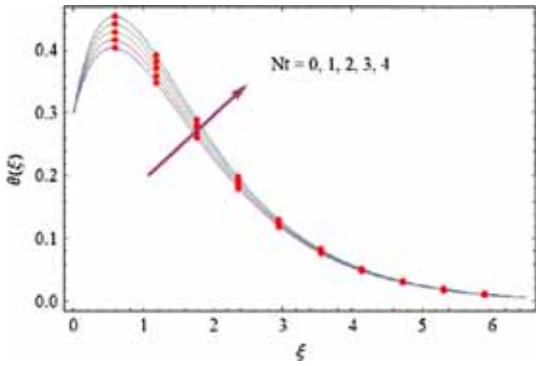

Figure 9. Impact of thermophoresis parameter (N_t) on temperature.

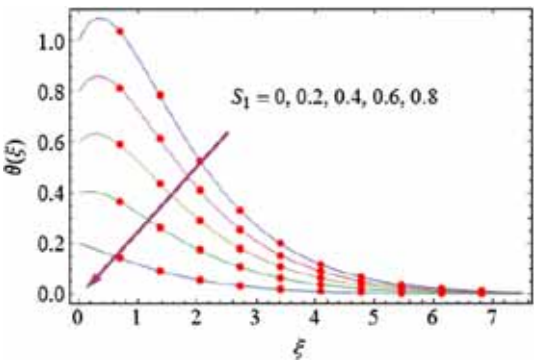

Figure 7. Impact of thermal stratification (S_1) on temperature.

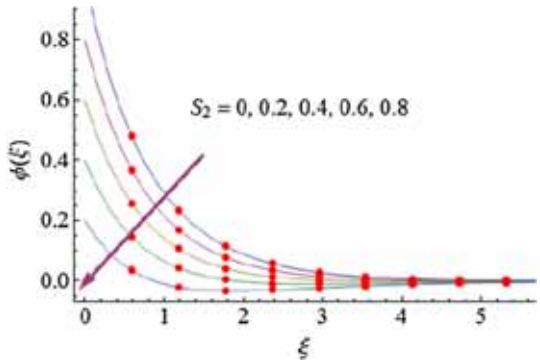

Figure 10. Impact of solutal stratification (S_2) on concentration.

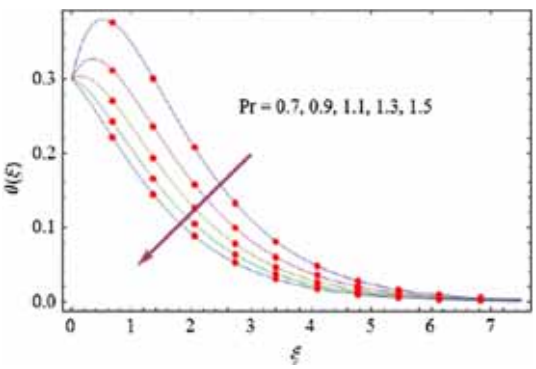

Figure 8. Impact of Prandtl number (Pr) on temperature.

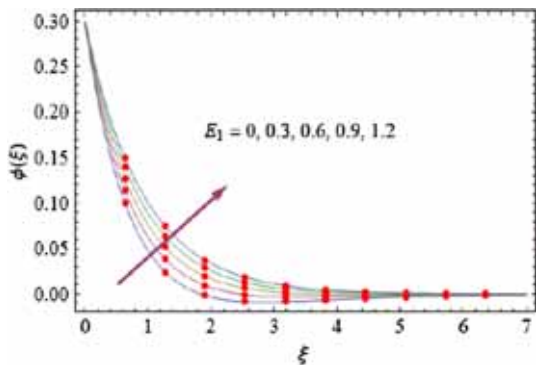

Figure 11. Impact of activation variable (E_1) on concentration.

this is due to the increase in relaxation time which is in direct relation with β_1. When there is a rise in relaxation time, the particles take more time to come back from the perturbed system to the equilibrium system. Figure 4 displays the impact of Deborah number with respect to the retardation time β_2 on $f'(\xi)$. For rising values of β_2 ($\beta_2 = 0, 0.4, 0.8, 1.2, 1.6$), the motion of the fluid particles increases. When there is an increase in β_2, the retardation time starts increasing due to which there is more disturbance in the system. Consequently, $f'(\xi)$ increases. The effect of magnetic parameter (M) on the velocity field is shown in figure 5. Lorentz force enhances for a larger estimation of M ($M = 0, 0.2, 0.4, 0.6, 0.8$) which produces resistance between the fluid particles due to which velocity $f'(\xi)$ decreases. Figure 6 is sketched to indicate the impact of the radiative parameter (R) on $\theta(\xi)$. It is noticed that the temperature of the fluid increases

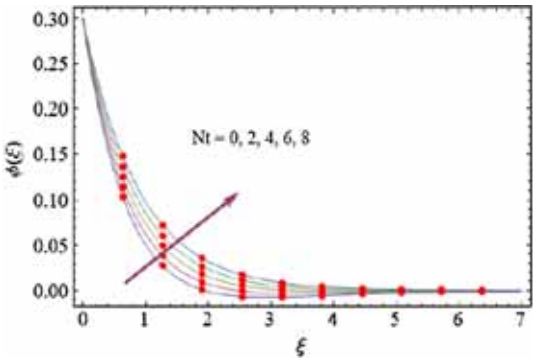

Figure 12. Impact of thermophoresis variable on concentration.

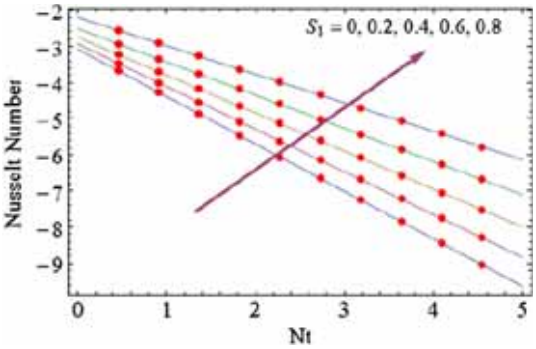

Figure 13. Impact of N_t and S_1 on Nusselt number.

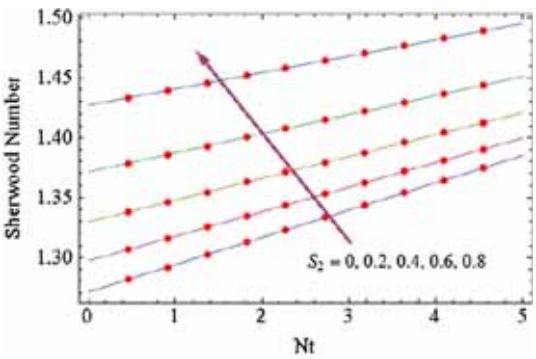

Figure 14. Impact of N_t and S_2 on Sherwood number.

for R ($R = 0, 0.1, 0.2, 0.3, 0.4$). Mean absorption coefficient decay for larger R occurs due to which temperature distribution $\theta(\xi)$ enhances. Figures 7 and 8 display the effect of thermal stratification parameter (S_1) and Prandtl number (Pr) on the temperature field ($\theta(\xi)$), respectively. Both have an opposite impact on temperature distribution ($\theta(\xi)$). Physically, for higher values of Pr (Pr $= 0.7, 0.9, 1.1, 1.3, 1.5$), the thermal conductivity of the fluid reduces, and so the temperature also decreases (see figure 8). Figure 9 shows the impact of thermophoresis parameter (N_t) on the temperature field ($\theta(\xi)$). An increasing trend of temperature is seen for a larger thermophoresis parameter N_t. Figure 10 delineates the impact of solutal stratification parameter (S_2) on the concentration field ($\phi(\xi)$). The concentration profile decreases for higher S_2 ($S_2 = 0, 0.2, 0.4, 0.6, 0.8$). Figure 11 shows the impact of activation variable E_1 on the concentration profile ($\phi(\xi)$). One can easily see the increment in $\phi(\xi)$ for $E_1 = 0, 0.3, 0.6, 0.9, 1.2$. For higher values of thermophoresis parameter N_t ($N_t = 0, 2, 4, 6, 8$), the concentration of the fluid enhances. Figure 13 displays the impact of thermophoresis (N_t) and thermal stratification (S_1) parameters on Nusselt number. It is seen that the magnitude of the Nusselt number decays for larger values of thermal stratification ($S_1 = 0, 0.2, 0.4, 0.6, 0.8$) while the opposite trend is noticed for larger thermophoresis (N_t). Figure 14 shows that the magnitude of the Sherwood number increases for both N_t and S_2.

7. Conclusions

The impact of activation energy in a nonlinear mixed convective flow of Oldroyd-B nanomaterial over a surface with variable thickness of stretchable sheets is analytically discussed in this communication. Expression of energy is mathematically modelled in the presence of radiative flux and a heat source/sink. Important slip mechanisms like Brownian and thermophoresis diffusion effects are considered. The obtained flow expressions are analytically solved using the OHAM. The individual residual error for the velocity, temperature and concentration fields is calculated using auxiliary variables. In our view, no such attempt is yet published in the literature to discuss the impact of activation energy on the nanomaterial flow of the Oldroyd-B fluid subject to nonlinear mixed convection, radiative flux, heat source/sink, surface with variable thickness, double stratification for both heat and mass transfer. The obtained results show that for increased values of Hartmann (magnetic parameter) and Deborah numbers, fluid velocity decreases. The temperature field shows an increasing behaviour for higher values of heat generation/absorption, radiative and temperature ratio parameters. Also Sherwood and Nusselt numbers increase with larger radiative and solutal stratified parameters.

References

[1] S Lee, S U Choi, S Li and J A Eastman, *J. Heat Transfer* **121**, 280 (1999)
[2] Y Xuan and Q Li, *J. Heat Transfer* **125**, 151 (2003)

[3] L Zhang, J Z Lv, M L Bai and D Guo, *Heat Transfer Eng.* **36**, 452 (2014)
[4] W Cui, M Bai, J Lv, G Li and X Li, *Ind. Eng. Chem. Res.* **50**, 13568 (2011)
[5] L Zhang, J Z Lv, M L Bai, Y N Bian, H Liu and S Q Shen, *J. Therm. Sci. Technol.* **1**, 1 (2014)
[6] R P Laein, S Rashidi and J A Esfahani, *Adv. Powder. Technol.* **27**, 312 (2016)
[7] T Hayat, K Muhammad, M I Khan and A Alsaedi, *Pramana – J. Phys.* **92**: 57 (2019)
[8] M I Khan, S Qayyum, T Hayat, M I Khan and A Alsaedi, *Int. J. Heat Mass Transf.* **133**, 959 (2019)
[9] W A Khan, A S Alshomrani, A K Alzahrani, M Khan and M Irfan, *Pramana – J. Phys.* **91**: 63 (2018)
[10] M I Khan, A Kumar, T Hayat, M Waqas and R Singh, *J. Mol. Liq.* **278**, 677 (2019)
[11] M I Khan, T Hayat, F Shah, M U Rahman and F Haq, *Int. J. Heat Mass Transf.* **135**, 561 (2019)
[12] M Kumar, G J Reddy and N Dalir, *Pramana – J. Phys.* **91**: 60 (2018)
[13] T Hayat, M Rashid, M I Khan and A Alsaedi, *Iran. J. Sci. Technol. Trans. A: Sci.* (2019), in press.
[14] M Khan, M Irfan and W A Khan, *Pramana – J. Phys.* **92**: 17 (2019)
[15] T Hayat, F Shah, M I Khan and A Alsaedi, *Results Phys.* **8**, 206 (2018)
[16] M I Khan, S Ullah, T Hayat, M Waqas, M I Khan and A Alsaedi, *Int. J. Heat Mass Transf.* **126**, 1337 (2018)
[17] T Hayat, M Waqas, S A Shehzad and A Alsaedi, *Pramana – J. Phys.* **86**, 3 (2016)
[18] M I Khan, T A Khan, S Qayyum, T Hayat, M I Khan and A Alsaedi, *Eur. Phys. J. Plus* **133**, 329 (2018)
[19] M I Khan, S Qayyum, T Hayat and A Alsaedi, *Chin. J. Phys.* **56**, 1525 (2018)
[20] T Hayat, M Z Kayani, A Alsaedi, M I Khan and I Ahmad, *Int. J. Heat Mass Transf.* **127**, 422 (2018)
[21] Z Odibat, *Appl. Numer. Math.* **137**, 203 (2019)
[22] T Hayat, M I Khan, M Farooq, A Alsaedi, M Waqas and T Yasmeen, *Int. J. Heat Mass Transf.* **99**, 702 (2016)
[23] M I Khan, M Waqas, T Hayat and A Alsaedi, *J. Colloid Interface Sci.* **498**, 85 (2017)
[24] T Hayat, M I Khan, S Qayyum and A Alsaedi, *Colloids Surf. A* **539**, 335 (2018)
[25] H Y Martínez and J F G Aguilar, *J. Comput. Appl. Math.* **346**, 247 (2019)
[26] M Azam, A Shakoor, H F Rasool and M Khan, *Int. J. Heat Mass Transf.* **131**, 495 (2019)
[27] M I Khan, T Hayat, M I Khan and A Alsaedi, *Int. Commun. Heat Mass Transf.* **91**, 216 (2018)
[28] S R Sheri and T Thumma, *Ain Shams Eng. J.* **9**, 1169 (2018)
[29] M I Khan, T Yasmeen, M I Khan, M Farooq and M Wakeel, *Renew. Sust. Energy Rev.* **66**, 702 (2016)
[30] T Ambreen, A Saleem and C W Park, *Powder Technol.* **345**, 509 (2019)
[31] N B Khan, Z Ibrahim, M I Khan, T Hayat and M F Javed, *Int. J. Heat Mass Transf.* **121**, 309 (2018)
[32] M Irfan, W A Khan, M Khan and M M Gulzar, *J. Phys. Chem. Solids* **125**, 141 (2019)
[33] M W A Khan, M I Khan, T Hayat and A Alsaedi, *Physica B* **534**, 113 (2018)
[34] T Hayat, M Tamoor, M I Khan and A Alsaedi, *Results Phys.* **6**, 1031 (2016)
[35] M N Rostami, S Dinarvand and I Pop, *Chin. J. Phys.* **56**, 2465 (2018)
[36] H Mirgolbabaee, S T Ledari, N M Zadeh and D D Ganji, *J. Taibah Univ. Sci.* **11**, 1110 (2017)
[37] H Mirgolbabaee, S T Ledari and D D Ganji, *Alexandria Eng. J.* **55**, 1695 (2016)
[38] S S Ghadikolaei, K Hosseinzadeh and D D Ganji, *Case Stud. Thermal Eng.* **10**, 579 (2017)
[39] H Mirgolbabaee, S T Ledari, M Sheikholeslami and D D Ganji, *Int. J. Appl. Comput. Math.* **3**, S1463 (2017)
[40] H Mirgolbabaee, S T Ledari and D D Ganji, *J. Assoc. Arab Univ. Basic Appl. Sci.* **24**, 213 (2017)
[41] M Danish, S Kumar and S Kumar, *Comput. Chem. Eng.* **36**, 57 (2012)
[42] T Hayat, T Nasir, M I Khan and A Alsaedi, *Results Phys.* **9**, 390 (2018)
[43] S Gupta, D Kumar and J Singh, *Int. J. Heat Mass Transf.* **118**, 378 (2018)
[44] A Alsaedi, M I Khan and T Hayat, *J. Theor. Comput. Chem.* **16**, 1750064 (2017)
[45] S J Liao, *Commun. Nonlinear Sci. Numer. Simul.* **15**, 2003 (2010)